

Spectro-temporal encoded Multiphoton Microscopy

Sebastian Karpf^{1,2*}, Carson Riche³, Dino di Carlo³, Anubhuti Goel⁴, William A. Zeiger⁴, Anand Suresh⁴, Carlos Portera-Cailliau⁴ and Bahram Jalali^{1,3}

¹Department of Electrical Engineering and Computational Science, University of California, Los Angeles (UCLA), Los Angeles CA-90095, USA

²Institute of Biomedical Optics (BMO), University Of Luebeck, 23562 Luebeck, Germany

³Department of Bioengineering, University of California, Los Angeles (UCLA), Los Angeles CA-90095, USA

⁴Department of Neurology, University of California, Los Angeles (UCLA), Los Angeles CA-90095, USA

*corresponding author: karpf@bmo.uni-luebeck.de

Two-Photon Microscopy¹ has become an invaluable tool for biological and medical research, providing high sensitivity, molecular specificity, inherent three-dimensional sub-cellular resolution and deep tissue penetration. In terms of imaging speeds, however, mechanical scanners still limit the acquisition rates to typically 10-100 frames per second. Here we present a high-speed non-linear microscope achieving kilohertz frame rates by employing pulse-modulated, rapidly wavelength-swept lasers and inertia-free beam steering through angular dispersion. In combination with a high bandwidth, single-photon sensitive detector, we achieve recording of fluorescent lifetimes at unprecedented speeds of 88 million pixels per second. We show diffraction-limited, multi-modal - Two-Photon fluorescence and fluorescence lifetime (FLIM) – microscopy and imaging flow cytometry with a digitally reconfigurable laser, imaging system and data acquisition system. These unprecedented speeds should enable high-speed and high-throughput image-assisted cell sorting.

The extension of regular one-photon fluorescence microscopy to non-linear two-photon microscopy (TPM)¹ has led to important applications, e.g., in brain research, where the advantages of deeper tissue penetration and inherent three-dimensional sectioning capability enable recording neuronal activity to interrogate brain function in living mice². Further, fluorescent lifetime imaging (FLIM)³ can probe internal biochemical interactions and external environment of molecules, e.g. for quantifying cellular energy metabolism in living cells^{4,5}. The quadratic dependency on intensity of TPM favours laser-scanning over

whole-field illumination, so typically raster-scanning with galvanometric mirrors is conducted. However, these mechanical mirrors are inertia limited to line-scan rates of <20kHz.

Here we report on a new approach of high-speed laser scanning in non-linear imaging using a rapidly wavelength swept laser in combination with a diffraction grating to achieve inertia-free, very rapid beam-scanning, orders of magnitude faster than mechanical scanners. We employ a high speed swept source Fourier-domain Mode-locked (FDML) laser⁶ which is modulated to short pulses and amplified to high peak powers. This FDML-MOPA laser was previously described in detail⁷. The swept wavelength output is sent onto a diffraction grating for line scanning (Fig. 1). Each pulse illuminates a distinct pixel both in time and in space (spectro-temporal encoding). The y-axis is scanned with a galvanometric mirror at typically 1kHz speed (slow axis). At an FDML sweep rate of 342 kHz this achieves a frame rate of 2 kHz for a 256x170 pixel frame size and 88 MHz pulse repetition rate. A high bandwidth detection at single-photon sensitivity enables recording of second harmonic generation (SHG), Two-Photon fluorescence and fluorescent lifetime (FLIM) at speeds of 88 million pixels per second. To the best of our knowledge, this is the highest achieved speed for both FLIM and two-photon FLIM ever reported.

This new microscope, which we coin spectro-temporal lifetime Imaging by diffracted excitation (SLIDE) microscope, can be digitally programmed to allow for adapting the pulse repetition rate to the fluorescent lifetimes. This is achieved through the direct pulse modulation through a 20 GHz bandwidth electro-optic modulator (EOM) (cf. Fig. 1 and our previous report⁷).

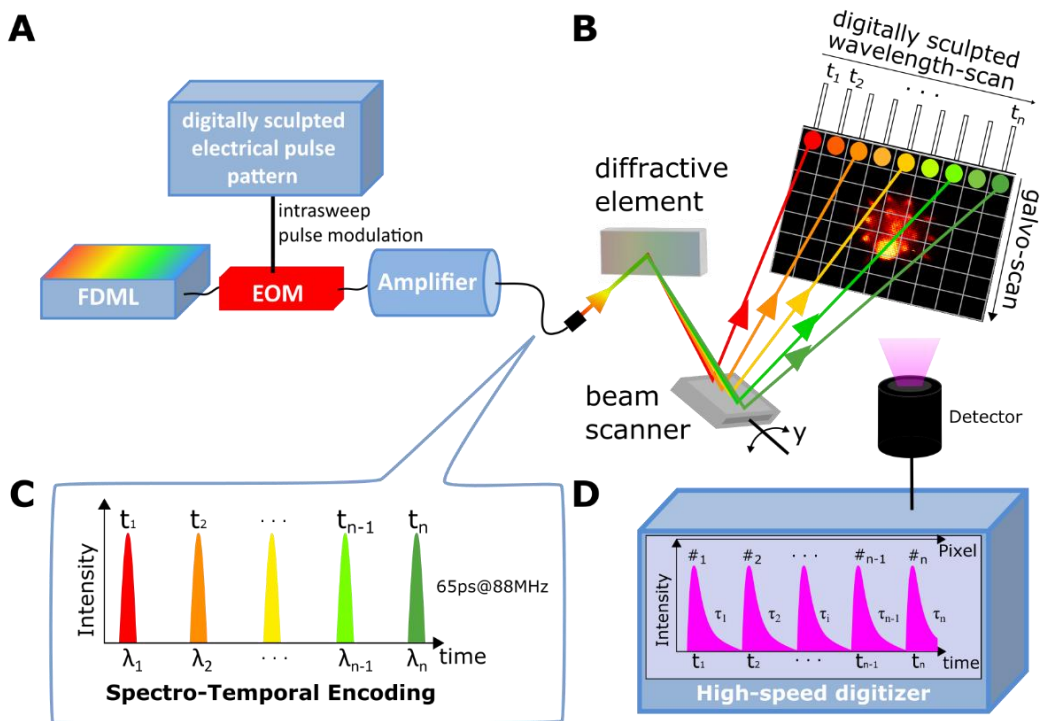


Figure 1 Principle of Spectro-temporal Lifetime Imaging by diffractive excitation (SLIDE). (A) A swept-source Fourier Domain Mode-Locked (FDML) laser is pulse-modulated, amplified and diffracted to produce rapid beam steering through spectrum-to-line mapping (B). The mapping pattern along each line is digitally shaped through the pulse modulation onto a fast electro-optic modulator (EOM). For raster-scanning the y-axis is scanned using a galvanometric scanner. (C) In SLIDE, each pulse has both a unique wavelength and time (spectro-temporal encoding) leading to a sequential and pixelwise illumination. (E) Fluorescence signals are recorded at high detection bandwidth to also enable fluorescent lifetime imaging (FLIM) at high speed.

Results

The experimental setup of the SLIDE microscope is presented in Figure 2. The whole system is electronically synchronized by an arbitrary waveform generator (AWG). It drives the FDML-MOPA laser including the pulse pattern, the y-axis galvo mirror and also the trigger and clock of the digitizer card. The modulated pulse length was measured to be 65ps (Fig. 2G). This pulse width corresponds to a time-bandwidth calculated linewidth of 25pm, so only a factor of two lower than the measured linewidth⁷. Raster scanning on the sample is achieved through spectro-temporal encoding along the x-axis and mechanical scanning on the y-axis (cf. Fig 1B). It shall be noted the used spectral bandwidth of 12nm (Fig. 2E) lies well within most Two-Photon absorption bandwidths, so equivalent fluorescence is excited along the whole line. The x-axis imaging resolution is given by the spectral resolution of the grating (67pm, see methods) and the

instantaneous laser linewidth (56pm, Fig. 2G). In combination with the swept bandwidth of 12nm, this should allow for $12\text{nm}/0.067\text{pm}\approx 180$ discernible spots, which we moderately oversample by programming 256 pulses along the x-direction. We tested the imaging resolution achieved through spectro-temporal encoding by imaging 200nm fluorescent beads and verified that diffraction limited imaging performance is achieved. We further verified that the fluorescence signal scales quadratically with the illumination power confirming Two-Photon origin of the signal. The instrument response function (IRF) of the detection was determined by SHG from a Urea sample and fitted to 1026ps (Fig. 2H). The analogue lifetime detection was investigated earlier to yield fluorescence lifetime values in agreement with literature values⁸ and enables rapid FLIM microscopy even at single pulse per pixel illumination (SP-FLIM)⁹.

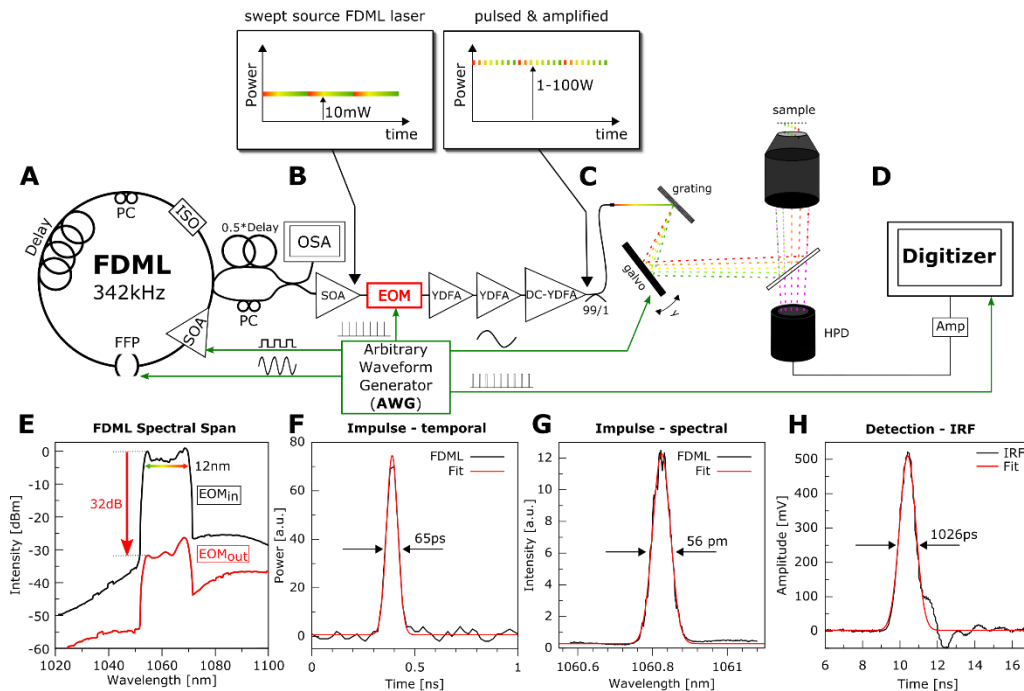


Figure 2 Experimental Setup of the SLIDE system. (A) The light source is an FDML-MOPA laser^{6,7} at 1060nm ($\pm 6\text{nm}$) and 342 kHz sweep repetition rate. Details on the laser can be found in a previous report.⁷ (C) The wavelength-swept laser is modulated by a digitally programmed pulse pattern which determines the line mapping in SLIDE. Typically each sweep (2.9 μs duration) is modulated to 256 impulses of short temporal width (65ps) to achieve a pixel rate of 88 MHz. This leaves enough time for most fluorescence transients to decay. The whole system is synchronized through an arbitrary waveform generator (AWG) which drives the FDML-MOPA laser⁷, the y-axis galvo and the digitizer card (trigger and sample clock). A high numerical aperture (NA) objective focuses the excitation light on the sample and collects the epi-generated fluorescence signal. A dichroic filter directs only non-linear signals on a fast hybrid photodetector (HPD), connected to a transimpedance amplifier and a fast digitizer (D). (E) A wavelength span of 12nm is used for spectral scanning. The EOM modulator achieves a high extinction ratio⁷ (~30 dB optical). (F) The recorded temporal pulse width achieved with the EOM is 65ps. (G) High-resolution pixel mapping is possible due to the narrow instantaneous linewidth of the pulsed FDML laser pulses measured to 56pm. (H) The instrument response function (IRF) of the detection was determined by SHG in a urea sample to 1026ps FWHM.

SLIDE imaging performance was assessed first by recording the field of view (FOV) on a resolution target (Fig. 3B). The x-axis was scanned with the spectro-temporal encoded scan while the y-axis was scanned with a galvanometric mirror (Fig. 3A). Figure 3C shows a Two-Photon microscopy image of a *euglena gracilis* microalgae and was recorded within 497 μ s at 2kHz frame rate. The time trace (Fig. 3D) of a single line illustrates the high SNR of up to 490 (peak SNR). This is due to the high photon counts achieved per excitation pulse (note that a single photon generates a voltage of 50mV). By zooming in on two individual pixels, we see a difference in the transient fluorescence decay time (Fig. 3F). To this end, 3x3 spatial binning was performed to yield enough fluorescent photons for a mono-exponential fit¹⁰. By fitting with the convoluted IRF a FLIM image can be generated (Fig. 3E) revealing two different domains within the algae cells. The autofluorescent chloroplasts decay fast and are color-coded red, while Nile red, an exogenous fluorophore which was added to highlight lipid generation within the microalgae, has a longer decay time and is color-coded green. Both imaging modalities TPM and FLIM are extracted from the same data which was acquired within 497 μ s for this 256x170 pixel image. Further imaging examples can be found in the supplementary material.

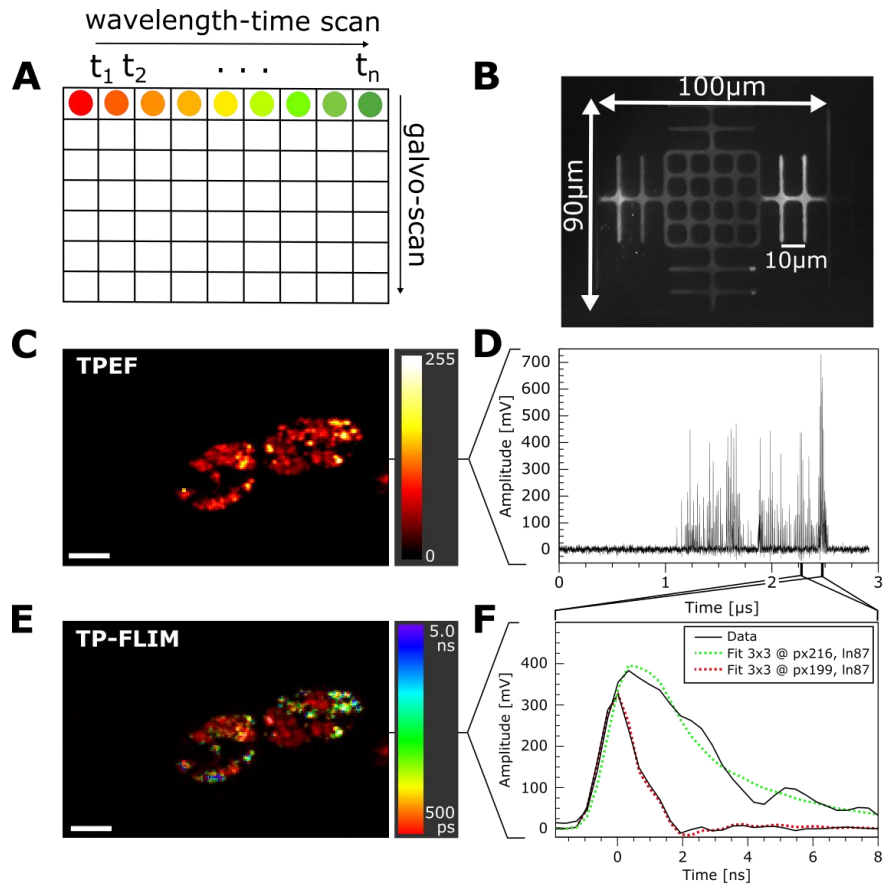


Figure 3 SLIDE high-speed dual-modality imaging at 2000 frames per second. (A) In SLIDE microscopy, the x-axis is scanned by spectro-temporal encoded diffraction scanning and the y-axis by a galvo mirror. (B) The field-of-view (FOV) is $100 \times 90 \mu\text{m}^2$ (resolution target has $10 \mu\text{m}$ pitch). (C) Two-Photon intensity image of *Euglena gracilis* algae cells (256×170 pixels). Each line is acquired within $2.9 \mu\text{s}$ at high signal-to-noise ratio (SNR) of up to 490 (peak SNR) (cf. D). Zooming into individual pixels (F) reveals different transient fluorescent decay times which can be fitted to extract a fluorescence lifetime value for each pixel. Therefore, a 3×3 pixel binning was applied for higher lifetime fidelity. The lifetimes are color-coded to achieve a TP-FLIM image (E) from the same dataset. In the TP-FLIM image the rapidly decaying autofluorescent chloroplasts (red) can be distinguished from the NileRed-stained lipid droplets (green, blue). This unaveraged image was acquired at 2.012 kHz frame-rate ($497 \mu\text{s}$ recording time). The average power on the sample was 30mW. Lifetimes were determined by deconvolution with the IRF (convolution fit shown in F). Photon counts for the curves in (F) are 82 photons (red) and 246 photons (green). Scale bar represents $10 \mu\text{m}$.

To calibrate the speed and accuracy of SLIDE we performed imaging flow cytometry of 5 different species of fluorescent beads (Fig. 4A,B). The beads range in size from 2 to $15 \mu\text{m}$ (similar to typical mammalian cell sizes) and Figure 4 nicely showcases that SLIDE imaging flow cytometry is capable of obtaining high quality images even at these high throughput rates of $>10,000$ objects per second. Fig. 4D₁-D₄ were acquired within $497 \mu\text{s}$ per image. Since these beads show high signal levels, analysis of the time domain data revealed that about 1-10 fluorescent photons were achieved per excitation pulse at 15mW average excitation power.

After 9x9 spatial binning was applied, photon counts were >100 photons per lifetime curve for reliable mono-exponential fitting¹⁰. For this application tail-fitting was applied to achieve fast fitting and test the accuracy. As can be seen by exemplary lifetime fits for all five beads shown in Figure 4C, the lifetime accuracy was still high, and the measured signals enabled high fidelity lifetime fits.

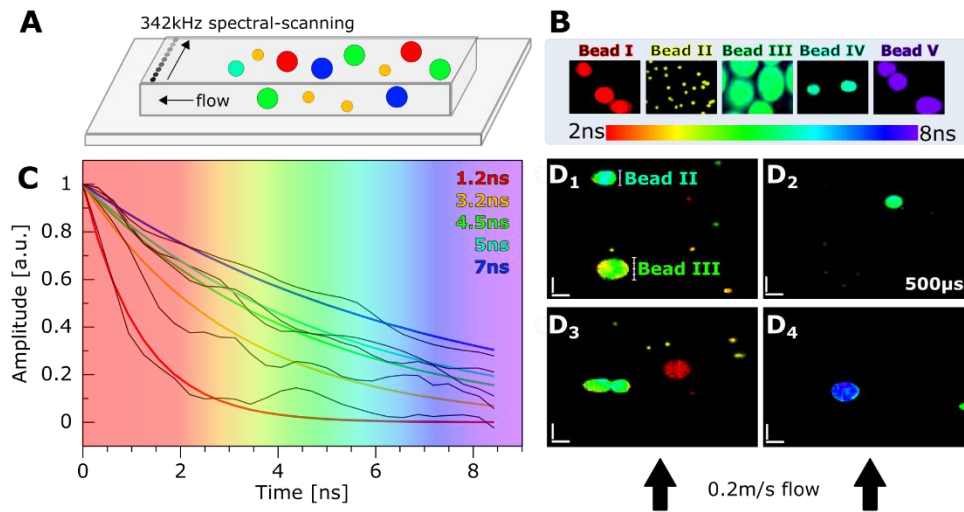


Figure 4 SLIDE Imaging flow cytometry at 0.2 m/s flow speed. (A) SLIDE line imaging was performed at 342 kHz line-scanning rate inside a flow channel. Only the direction perpendicular to the flow was scanned via SLIDE, while the flow speed gives the scanning in the y-axis direction. (B) Five different calibration fluorescent beads were first imaged at rest to obtain reference lifetime colours. Subfigure B shows averaged SLIDE images (1000-times averaging). The lifetimes range from 2-8ns (B,C). Afterwards, a mixture of all beads was imaged in flow at flow speeds of 0.2 m/s in order to obtain even sampling period in both dimensions at 550nm pitch (see methods). The five different species show different lifetimes (C) and can be clearly distinguished via TP-FLIM (D₁-D₄) even at these high flow speeds. Sample throughput is estimated to be >10.000 beads per second. Images were generated with 170 vertical lines, so each image D₁-D₄ was recorded within 497 µs. The images have high SNR and high resolution. For lifetime accuracy, 9x9 pixel binning was applied to yield >100 photons per fluorescence lifetime decay to allow for reliable mono-exponential lifetime fits¹⁰. The pixel rate was 88MHz, i.e. single excitation pulse per pixel without averaging. The power used was 15mW, scale bars represent 10µm.

As a biological sample we imaged *Euglena gracilis* cells in SLIDE imaging flow cytometry mode, where autofluorescence from chloroplasts revealed a short fluorescence lifetime and Nile Red stained lipids show a longer lifetime (see also Fig. 3). Figure 5 presents four different snapshots of *Euglena gracilis* microalgae in flow where each image pair (Two-Photon & Two-Photon FLIM images) was acquired within 1ms. The TPM images already shows the high-resolution which reveals sub-cellular morphology. Yet, through the FLIM images it is possible to discern chloroplasts from lipids through their fluorescent lifetime. The images have very high resolution and high SNR and, even though they were obtain at very high speeds in flow,

they have quality comparable to regular one-photon fluorescence microscopy¹¹. Excitation power was 30mW on the sample and 5x5 pixel spatial binning was applied to ensure >100 photons per lifetime curve. Fluorescence lifetime can aid in discerning lipids as it is independent of concentration and signal height. This high-speed lipid content screening by SLIDE FLIM cytometry may help in purification of high lipid content microalgae for efficient biofuel production¹¹.

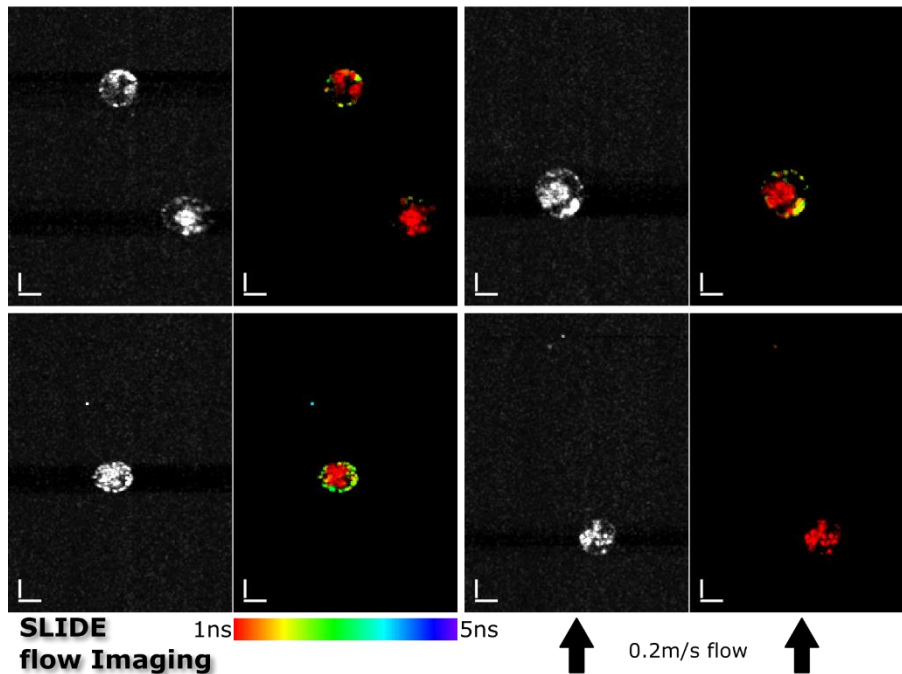


Figure 5 SLIDE Lifetime Imaging flow cytometry of *Euglena gracilis* algae cells at 0.2 m/s flow speed. The Nile Red stained lipids can be clearly distinguished from the autofluorescent chloroplasts by their longer fluorescent lifetime (~5ns and ~1ns, respectively, cf. Fig. 3), even at these high flow rates. High subcellular resolution is achieved and morphologic structure as well as molecular information is recorded by SLIDE imaging flow cytometry. The displayed images have 256x342 pixels resolution which corresponds to a recording time of only 1ms per image pair (TPM left, SP-FLIM⁹ right). In the FLIM images a 5x5 spatial binning was applied to ensure >100 photons per fluorescence lifetime decay. The power used was 30mW, scale bars represent 10µm.

Discussion:

It shall be noted that the high speeds achieved by SLIDE require bright samples in order to detect many fluorescence photons per excitation pulse. However, not all samples provide enough fluorophores in the focal volume, such as genetically encoded fluorescent proteins. We tested imaging of genetically encoded tdTomato fluorescent proteins in *ex vivo* mouse brain to test whether a kHz frame-rate could be achieved in imaging neuronal activity. However, even though we were able to obtain morphological images (see

supplementary images), we found that only single fluorescent proteins were present in the focal volume and the signal was saturated, as increasing the laser power did not yield a quadratic signal increase. This does not permit recording neuronal ensemble activity at the kHz speed of the SLIDE systems, as both fluorescence intensity changes or fluorescence lifetime changes require tens to hundreds of photons thus sacrificing the speed as a result of averaging. Therefore, biochemically engineered fast and bright fluorescent proteins are needed, which can also be expressed at high abundance without interfering with cellular behaviour, in order to enable kHz frame-rate imaging of neuronal activity for SLIDE or any other fast technique in the future.

It is noted that SLIDE microscopy employs higher average powers (~ 10 - 100 mW) compared to conventional two-photon microscopes (1 - 30 mW) and this is due to the fast acquisition rates obtained by SLIDE together with the relatively longer pulse length. However, we did not notice any sample damage. This may be due to the longer wavelength¹², or the lower effective repetition rate per pixel and longer pulse length which was found to drastically reduce photobleaching^{13,14}. In fact, the effective repetition rate per pixel of only 1 kHz in SLIDE permits relaxation of even long lived triplet states¹³. Further, we hypothesize that SLIDE profits from the linear pulse length dependency of TPM⁸, since, to increase photon numbers per single pulse it may practically be advantageous to rather increase the pulse length than the peak power in order to avoid supra-quadratic scaling effects like photobleaching¹⁴ and photodamage¹⁵. Lastly, even though pulse energies become larger with longer pulses, photothermal effects on the sample are insignificant in SLIDE microscopy as they are negligibly small¹⁶ and dissipate in between frame scans.

Regarding sensitivity, Figures 3 and 4 also show that SLIDE has sensitivity down to the single molecule level, so even samples where only a single fluorescent emitter is excited in the focal volume can be successfully imaged with SLIDE. In this sparse signal case, required photon counts can be reached either by spatial binning or, in applications where high spatial resolution FLIM is required⁵, by phase-locked detection and averaging. In SLIDE, frame averaging can be performed at low effective pulse repetition rate per pixel which can help increase signal levels¹⁷.

Conclusion

In this manuscript we presented the concept of high-speed SLIDE microscopy along with the experimental implementation and application in Two-Photon imaging flow cytometry with two imaging modalities, TPM and FLIM. Record high speeds of 342 kHz line scanning rates and 88 MHz lifetime pixel rates were presented. This corresponds to FLIM pixel dwell times of only 11 nanosecond, which – to the best of our knowledge – represent the fastest FLIM recordings ever presented. This speed is orders of magnitudes faster than what is achievable with TCSPC-based systems. We presented high quality fluorescence lifetime imaging flow cytometry at very high speeds (>10,000 events per second). We believe that this high throughput and multi-modality enabled by SLIDE microscopy can lead to new insights into rapid biological processes and detection of rare events in applications like liquid biopsy or rare circulating tumour cell detection¹⁸. Further, the fiber-based setup of the SLIDE microscopy system may enable an endoscopic application to overcome the relatively shallow penetration depth of optical microscopy.

Acknowledgement: This research was sponsored in part by the National Institutes of Health grants 5R21GM107924-03 to BJ and CP-C and R21EB019645 to BJ, Cal-BRAIN grant 350050 (California Blueprint for Research to Advance Innovations in Neuroscience) to BJ and CP-C, as well as grant W81XWH-14-1-0433 (USAMRMC, DOD), and NIH NICHD grant R01 HD054453 to CP-C. Sebastian Karpf gratefully acknowledges a Postdoctoral research fellowship from the German Research Foundation (DFG, project KA 4354/1-1).

Author Contributions: S.K. conceived the idea, built the system and conducted the experiments. C.R. and D.d.C. provided the *Euglena gracilis* cells. C.R. and S.K. conducted the *Euglena* flow measurements. A.G, W.Z., A. S. and C.P.C. provided the mouse brain sample. C.P.C. and S.K. conducted the mouse brain imaging measurement. S.K. and B.J. conceived the digital image processing capabilities. B.J. and S.K. performed system analysis and wrote the manuscript. B.J. supervised the research.

Reference List

- 1 Denk, W., Strickler, J. & Webb, W. Two-photon laser scanning fluorescence microscopy. *Science* **248**, 73-76, doi:10.1126/science.2321027 (1990).
- 2 Gong, Y. *et al.* High-speed recording of neural spikes in awake mice and flies with a fluorescent voltage sensor. *Science* **350**, 1361-1366, doi:10.1126/science.aab0810 (2015).
- 3 Lakowicz, J. R., Szmacinski, H., Nowaczyk, K., Berndt, K. W. & Johnson, M. Fluorescence lifetime imaging. *Analytical Biochemistry* **202**, 316-330, doi:[http://dx.doi.org/10.1016/0003-2697\(92\)90112-K](http://dx.doi.org/10.1016/0003-2697(92)90112-K) (1992).
- 4 Blacker, T. S. *et al.* Separating NADH and NADPH fluorescence in live cells and tissues using FLIM. *Nature Communications* **5**, 3936, doi:10.1038/ncomms4936 (2014).
- 5 Evers, M. *et al.* Enhanced quantification of metabolic activity for individual adipocytes by label-free FLIM. *Scientific Reports* **8**, 8757, doi:10.1038/s41598-018-27093-x (2018).
- 6 Huber, R., Wojtkowski, M. & Fujimoto, J. G. Fourier Domain Mode Locking (FDML): A new laser operating regime and applications for optical coherence tomography. *Opt. Express* **14**, 3225-3237, doi:10.1364/OE.14.003225 (2006).
- 7 Karpf, S. & Jalali, B. Fourier-domain mode-locked laser combined with a master-oscillator power amplifier architecture. *Opt. Lett.* **44**, 1952-1955, doi:10.1364/OL.44.001952 (2019).
- 8 Karpf, S. *et al.* Two-photon microscopy using fiber-based nanosecond excitation. *Biomed. Opt. Express* **7**, 2432-2440, doi:10.1364/BOE.7.002432 (2016).
- 9 Eibl, M. *et al.* Single pulse two photon fluorescence lifetime imaging (SP-FLIM) with MHz pixel rate. *Biomed. Opt. Express* **8**, 3132-3142, doi:10.1364/BOE.8.003132 (2017).
- 10 Köllner, M. & Wolfrum, J. How many photons are necessary for fluorescence-lifetime measurements? *Chemical Physics Letters* **200**, 199-204, doi:[https://doi.org/10.1016/0009-2614\(92\)87068-Z](https://doi.org/10.1016/0009-2614(92)87068-Z) (1992).
- 11 Yamada, K. *et al.* Efficient selective breeding of live oil-rich *Euglena gracilis* with fluorescence-activated cell sorting. *Scientific Reports* **6**, 26327, doi:10.1038/srep26327 <https://www.nature.com/articles/srep26327#supplementary-information> (2016).
- 12 Chen, S.-Y. *et al.* In Vivo Virtual Biopsy of Human Skin by Using Noninvasive Higher Harmonic Generation Microscopy. *Selected Topics in Quantum Electronics, IEEE Journal of* **16**, 478-492, doi:10.1109/JSTQE.2009.2031987 (2010).
- 13 Donnert, G., Eggeling, C. & Hell, S. W. Major signal increase in fluorescence microscopy through dark-state relaxation. *Nat Meth* **4**, 81-86 (2007).
- 14 Patterson, G. H. & Piston, D. W. Photobleaching in Two-Photon Excitation Microscopy. *Biophysical Journal* **78**, 2159-2162, doi:[http://dx.doi.org/10.1016/S0006-3495\(00\)76762-2](http://dx.doi.org/10.1016/S0006-3495(00)76762-2) (2000).
- 15 Hopt, A. & Neher, E. Highly Nonlinear Photodamage in Two-Photon Fluorescence Microscopy. *Biophysical Journal* **80**, 2029-2036, doi:[http://dx.doi.org/10.1016/S0006-3495\(01\)76173-5](http://dx.doi.org/10.1016/S0006-3495(01)76173-5) (2001).
- 16 Schönle, A. & Hell, S. W. Heating by absorption in the focus of an objective lens. *Opt. Lett.* **23**, 325-327, doi:10.1364/OL.23.000325 (1998).
- 17 Chen, X., Leischner, U., Rochefort, N. L., Nelken, I. & Konnerth, A. Functional mapping of single spines in cortical neurons in vivo. *Nature* **475**, 501-505, doi:10.1038/nature10193 (2011).
- 18 He, W., Wang, H., Hartmann, L. C., Cheng, J.-X. & Low, P. S. In vivo quantitation of rare circulating tumor cells by multiphoton intravital flow cytometry. *Proceedings of the National Academy of Sciences* **104**, 11760-11765, doi:10.1073/pnas.0703875104 (2007).
- 19 Boudoux, C. *et al.* Rapid wavelength-swept spectrally encoded confocal microscopy. *Opt. Express* **13**, 8214-8221, doi:10.1364/OPEX.13.008214 (2005).

- 20 Goda, K., Tsia, K. K. & Jalali, B. Serial time-encoded amplified imaging for real-time observation of fast dynamic phenomena. *Nature* **458**, 1145-1149, doi:http://www.nature.com/nature/journal/v458/n7242/supinfo/nature07980_S1.html (2009).
- 21 Chen, C. L. *et al.* Deep Learning in Label-free Cell Classification. *Scientific Reports* **6**, 21471, doi:<http://dx.doi.org/10.1038/srep21471> (2016).
- 22 Bhushan, A. S., Coppinger, F. & Jalali, B. Time-stretched analogue-to-digital conversion. *Electronics Letters* **34**, 839-841, doi:10.1049/el:19980629 (1998).
- 23 Lechleiter, J. D., Lin, D.-T. & Sieneart, I. Multi-Photon Laser Scanning Microscopy Using an Acoustic Optical Deflector. *Biophysical Journal* **83**, 2292-2299, doi:[http://dx.doi.org/10.1016/S0006-3495\(02\)73989-1](http://dx.doi.org/10.1016/S0006-3495(02)73989-1) (2002).
- 24 Bewersdorf, J., Pick, R. & Hell, S. W. Multifocal multiphoton microscopy. *Opt. Lett.* **23**, 655-657, doi:10.1364/OL.23.000655 (1998).
- 25 Kim, K. H. *et al.* Multifocal multiphoton microscopy based on multianode photomultiplier tubes. *Opt. Express* **15**, 11658-11678, doi:10.1364/OE.15.011658 (2007).
- 26 Cheng, A., Goncalves, J. T., Golshani, P., Arisaka, K. & Portera-Cailliau, C. Simultaneous two-photon calcium imaging at different depths with spatiotemporal multiplexing. *Nat Meth* **8**, 139-142, doi:<http://www.nature.com/nmeth/journal/v8/n2/abs/nmeth.1552.html#supplementary-information> (2011).
- 27 Klein, T. & Huber, R. High-speed OCT light sources and systems [Invited]. *Biomed. Opt. Express* **8**, 828-859, doi:10.1364/BOE.8.000828 (2017).
- 28 Wieser, W. *et al.* High definition live 3D-OCT in vivo: design and evaluation of a 4D OCT engine with 1 GVoxel/s. *Biomed. Opt. Express* **5**, 2963-2977, doi:10.1364/BOE.5.002963 (2014).
- 29 Eigenwillig, C. M. *et al.* Picosecond pulses from wavelength-swept continuous-wave Fourier domain mode-locked lasers. *Nat Commun* **4**, 1848, doi:10.1038/ncomms2870 (2013).
- 30 Karpf, S., Eibl, M., Wieser, W., Klein, T. & Huber, R. A Time-Encoded Technique for fibre-based hyperspectral broadband stimulated Raman microscopy. *Nature Communications* **6**, 6784, doi:10.1038/ncomms7784 (2015).
- 31 Yokoyama, H. *et al.* Two-photon bioimaging with picosecond optical pulses from a semiconductor laser. *Opt. Express* **14**, 3467-3471, doi:10.1364/OE.14.003467 (2006).
- 32 Débarre, D., Olivier, N., Supatto, W. & Beaurepaire, E. Mitigating Phototoxicity during Multiphoton Microscopy of Live *Drosophila* Embryos in the 1.0–1.2 μm Wavelength Range. *PLOS ONE* **9**, e104250, doi:10.1371/journal.pone.0104250 (2014).
- 33 König, K., Becker, T. W., Fischer, P., Riemann, I. & Halhuber, K. J. Pulse-length dependence of cellular response to intense near-infrared laser pulses in multiphoton microscopes. *Opt. Lett.* **24**, 113-115, doi:10.1364/OL.24.000113 (1999).
- 34 Koren, L. E. High-yield media for photosynthesizing *Euglena gracilis* Z. *J. Protozool.* **14**, 17 (1967).

Methods:

Spectro-temporal encoded information

Enhancing imaging speeds through spectral-encoded scanning has been successfully employed for confocal microscopy¹⁹, high-speed brightfield imaging²⁰, quantitative phase imaging²¹ and more especially by employing the time stretch technique²⁰⁻²². However, these approaches could not be used for fluorescence imaging, as both the emission spectrum and the fluorescent lifetime are governed by the fluorescing molecule, so the original spectral encoding is lost upon the fluorescence emission. Therefore, in SLIDE, further temporal encoding from the wavelength swept laser is harnessed to achieve spectro-temporal encoded imaging. The wavelength is used for high-speed inertia-free point scanning and the temporal encoding for one-to-one mapping of the signal to the imaging pixels like in conventional raster-scanning or laser scanning microscopy. Spectro-temporal encoded imaging has unique advantages over other high-speed non-linear imaging approaches^{17,23-26} in terms of resolution, lifetime modality, compactness, flexibility, and fiber-based setup.

Time Bandwidth Product in Spectro-temporal Lifetime Imaging via Digitally Shaped Excitation (SLIDE)

Spectro-temporal encoding with high information density places rigorous requirements on the spectro-temporal bandwidth of the light source. The wavelength sweep time ΔT is equal to the number of pixels n times the time between pulses Δt_i , governed by the information-interrogation induced latency (here: fluorescent decay time τ_i). Considering, for example, 256 horizontal (linescan) pixels and a typical total fluorescent decay time of 10ns, this time calculates to $\Delta T = 2.56\mu\text{s}$. Assuming a spectral resolution of $\Delta\lambda_i = 100\text{pm}$ for the diffractive mapping means that the light source needs to sweep over $\Delta\lambda = 25.6\text{nm}$ in $\Delta T = 2.56\mu\text{s}$. A unique feature in SLIDE is that the spectro-temporal bandwidth scales quadratically with the number of pixels (in linescan):

$$\text{Spectro-temporal bandwidth } M_{\text{ST}} = \Delta T \times \Delta\lambda = n^2 \times \Delta\lambda_i \times \Delta t_i$$

A wavelength tuning speed of tens of nm over few microseconds is beyond the reach of conventional tuneable lasers^{6,27}. Although very fast tuning speeds can be achieved by chirping a supercontinuum pulse source in a dispersive medium as employed in time stretch techniques, achieving a time span of 2.56 μ s is about three orders of magnitude beyond the reach of available dispersive elements (typically in the ns-regime). Furthermore, the spreading of energy due to the stretching would result in negligible peak powers and would prevent non-linear excitation.

Spectro-temporal stretch via an FDML laser solves this predicament. The FDML laser provides a combination of large spectral span along with microseconds time span and narrow instantaneous linewidth. This novel type of laser has mainly been used for fast optical coherence tomography (OCT)^{6,27,28}, semiconductor compressed pulse generation²⁹ and non-linear stimulated Raman microscopy³⁰. Its low instantaneous linewidth allows us to achieve diffraction-limited spatial resolution a feat that is not possible with chirped supercontinuum sources.

Picosecond Excitation Pulses for rapid lifetime imaging

Our fast lifetime imaging capability is possible by the direct analogue recording of the fluorescent lifetime decay and is further enhanced by the higher number of photons generated per pulse by picosecond excitation pulses^{8,31}, enabling single pulse per pixel illumination. This has a number of advantages over traditional illumination: (i) A single pulse per pixel leads to a very low effective repetition rate per pixel, equal to the frame-rate (approx. 2kHz). This has been shown to decrease photobleaching and thereby increasing the signal levels¹³. In fact, even when averaging is desired, e.g. for double-exponential lifetime fits, it may be advantageous to average 2000 frames obtained with SLIDE within 1 second, to applying 2000 pulses per pixel at a pixel dwell time of 23 μ s and then raster-scanning the image in 1 second. (ii) Longer pulses lead to reduced pulse peak powers at same SNR, thus having the advantage of avoiding higher-than-quadratic effects like photobleaching^{13,14} and photodamage^{15,32,33} (scale at orders >2). Further, time-scales for intersystem crossing (ISC) are longer than the pulse length employed here, so no further

excitation from the triplet state should occur within the same pulse. (iii) The longer pulses are generated by digitally synthesized EO modulation which renders the excitation pattern freely programmable. For example, for optimal detection the pixel rate can be tailored to the fluorescence lifetime of the sample and allows warped (anamorphic) spatial illumination that takes advantage of sparsity to achieve optical data compression. (iv) Longer pulses generate quasi-monochromatic light and this renders the high-speed line-scanning spectral mapping by diffraction gratings possible. (v) The quasi-monochromatic light is optimally compatible with fibre delivery by omitting chromatic dispersion and pulse spreading. The excitation laser presented here is already fully fibre-based, making a future implementation into a multi-photon endoscope straight forward.

Wavelength-to-space Mapping

Upon exiting the single-mode fibre, the light was collimated using an $f=37$ mm lens followed by a beam-expander ($f=100$ mm and $f=150$ mm). This results in a beam diameter of 11.5mm filling the 60x microscope objective aperture. The grating was positioned at a 30° angle, such that the first order was reflected at almost the incident direction in order to minimize ellipticity of the first-order diffraction beam. At 1200 lines/mm the grating only produced a 0 and +1 diffraction order and the first order power was maximized by adjusting the polarization on a polarization control paddle. The grating resolution is calculated to 67pm. This fits well to the instantaneous linewidth of the FDML, which was measured for a single pulse to be 56pm (cf. Fig. 2).

Microscopy Setup

Two lenses were used to relay image the beams onto a galvanometric mirror (Cambridge Technology) for y-axis scanning. The galvo mirror was driven synchronously, producing 170 lines at 2.012 kHz. A high NA, oil immersion microscope objectives was used (Nikon Plan Apo 60x NA 1.4 oil). The field-of-view (FOV) was determined by inserting a resolution target and recording the reflected excitation light on a CCD camera installed in the microscope, which was sensitive to the 1064nm excitation light (cf. Figure 3). A dichroic

mirror (Thorlabs DMSP950R) in combination with an additional short-pass optical filter (Semrock FF01-750) transmits the Epi-generated signals to a hybrid Photodetector (HPD, Hamamatsu R10467U-40) with high quantum efficiency (45%). The high time resolution of the HPD in combination with a fast digitizer ($\sim 3\text{GS/s}$) leads to a fast instrument response function (IRF) of only 1026ps, measured by detecting the instantaneous signal of SHG in urea crystals (cf. Fig 2).

Digitally synthesized waveforms

The whole system is driven by an arbitrary waveform generator (AWG, Tektronix AWG7052). This AWG provides all digitally synthesized driving waveforms, driving the FDML laser (Fabry-Pérot Filter waveform and 50% modulation of SOA for buffering), the galvo-mirror and also generates an external sample clock signal for the digitizer. The waveforms are digitally programmed and enable flexibility on the number of pulses per sweep, pulse width, pulse shape, pulse pattern and thus also the image sampling density.

Digitizer

As digitizers, either an oscilloscope (Tektronix DPO71604B) at 3.125 GSamples/s or a streaming ADC card (Innovative Integrations Andale X6GSPS and Alazartech ATS9373) with synchronously driven sample clock at 3196MHz or 3940MHz, respectively, were employed. The external sample clock was employed such that the data acquisition runs synchronously to the FDML laser and the pulse modulation and ensures sample-accurate fitting. In order to acquire large data sets, a streaming ADC in combination with a RAID-SSD array was employed to store the data.

Flow cytometry

In the flow cytometry recording, the flow-rate was set by two fundamental properties, namely the fluorescence lifetime and the imaging diffraction limit. The lifetime limits the repetition rate to $\sim 100\text{MHz}$, while the diffraction limit is sampled at $\sim 380\text{nm}$. Consequently, we employed 88MHz repetition rate at 256 pulses per 2.92 μs linescan rate and 100 μm field-of-view. The flow rate was equally set to sample each line at 380nm, i.e. $380\text{nm}/2.92\mu\text{s}=0.13\text{m/s}$. The scale bars in the flow cytometry images were generated

using the known 10 μ m size of the Red-species bead to calibrate the actual flow speed. The Red bead was sampled with 18 lines, calculating to a line spacing of 556nm. Using the line scan rate of 342kHz, this calculates to a flow speed of \sim 0.2m/s.

Data Processing

For precise measurements, a deconvolution with the IRF was conducted in order to extract the fluorescent lifetimes (e.g. in Fig. 3). However, this is time consuming, so for faster processing and qualitative results a tail-fitting algorithm was used. Often time, different species need to be discerned so a qualitative value is sufficient. Photon numbers were calculated by dividing the area under the curve by the area of a single-photon event. For all images, the data was processed and images created in LabVIEW. The 2P-FLIM images were generated as HSL-images, where Hue was given by the lifetime-values, lightness by the integrated TPEF signal and saturation always set to maximum, i.e. the same for all images. For the TPEF images, the “Red Hot” or “Royal” look-up tables were applied in ImageJ. The plots were generated in GNUPlot and the figures produced using Inkscape.

Samples

The Pollen grain samples were ordered from Carolina (B690 slide) and the acridine orange stained *convallaria majalis* (lily of the valley flower stem) from Lieder GmbH, Germany. The fluorescent beads were ordered from ThermoFisher Scientific (# F8825, F8839, F8841, F8843, and F21012).

Experimental model systems: Euglena cell culture and fermentation

The *E. gracilis* cells used in the study are *Euglena gracilis* Z (NIES-48) strain procured from the Microbial Culture Collection at the National Institute for Environmental Studies (NIES), Japan. *E. gracilis* and were cultured heterotrophically in 500 mL flasks using Koren-Hutner (KH) medium at a pH of 3.5³⁴. The cell cultures were maintained at 23 °C with a shaking rate of 120 strokes/min under continuous illumination of 100 μ mol photons m⁻² s⁻¹. Cells were subjected to anaerobic

fermentation to induce lipid accumulation. The fermentation was performed on cells in stationary phase by bubbling with nitrogen gas and incubating the flasks in the dark for three days.

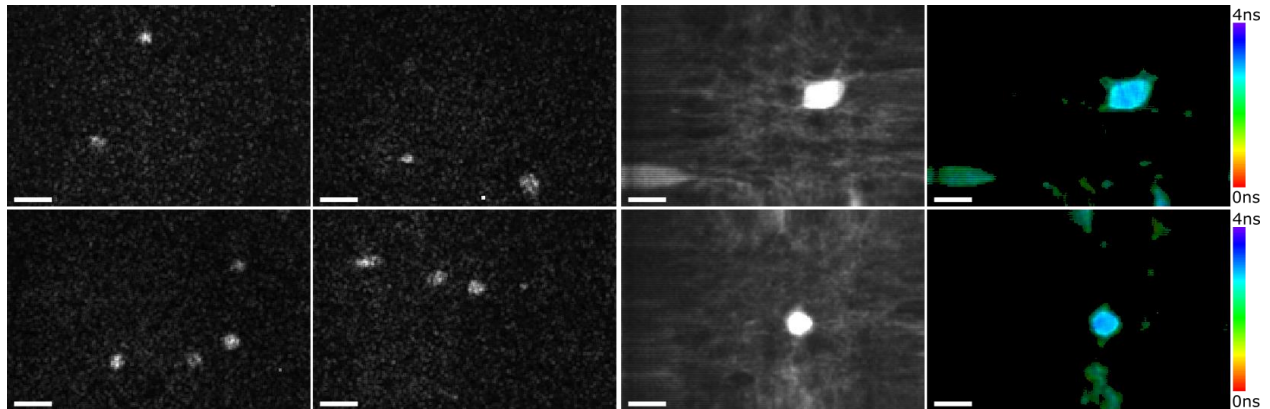
Nile red staining of intracellular lipid droplets

The Nile red stock was prepared by dissolving original dye powder (Sigma) into 4 mL dimethyl sulfoxide (DMSO) to achieve a concentration of 15.9 mg/mL (50 mM). The stain stock solution was diluted 1,000 times with distilled water before use. The *E. gracilis* cells in the culture medium were washed with distilled water and resuspended in distilled water with a final concentration of 2×10^6 cells/mL. We mixed 15.9 $\mu\text{g/mL}$ of Nile red solution with *E. gracilis* cell suspension solution at a volume ratio of 1:1, which was followed by gentle vibration and incubation in the dark for 10 min. The final concentration of Nile red and *E. gracilis* cells were 7.95 $\mu\text{g/mL}$ and 1×10^6 cells/mL, respectively. The *E. gracilis* cells were washed three times with distilled water and centrifugation (2000 x g, 1 min). The cells were resuspended in distilled water and protected from light prior to imaging.

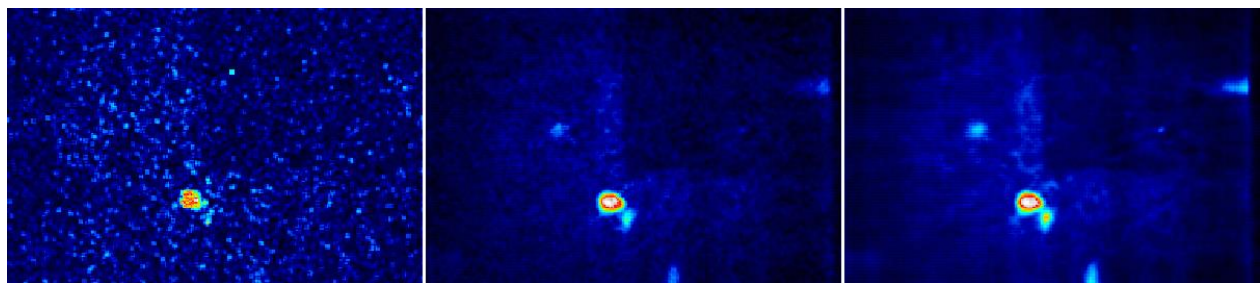
Experimental model systems: Mice brain imaging

All experiments followed the U.S. National Institutes of Health guidelines for animal research, under an animal use protocol (ARC #2007-035) approved by the Chancellor's Animal Research Committee and Office for Animal Research Oversight at the University of California, Los Angeles. Experiments in Supplementary materials used FVB.129P2 wild-type mice (JAX line 004828). Two weeks after viral injection, mice expressing TdTomato were perfused intracardially with 4% paraformaldehyde in phosphate buffer and their brains were extracted and glued on a petri dish, which was filled with PBS buffer for imaging on the inverted microscope. Neurons expressing TdTomato were imaged in Layer 2/3 at a depth of ~150-250 μm below the dura using a long working range 40x microscope objective (Nikon N40X-NIR - 40X Nikon CFI APO NIR Objective, 0.80 NA, 3.5 mm WD).

Supplementary Information

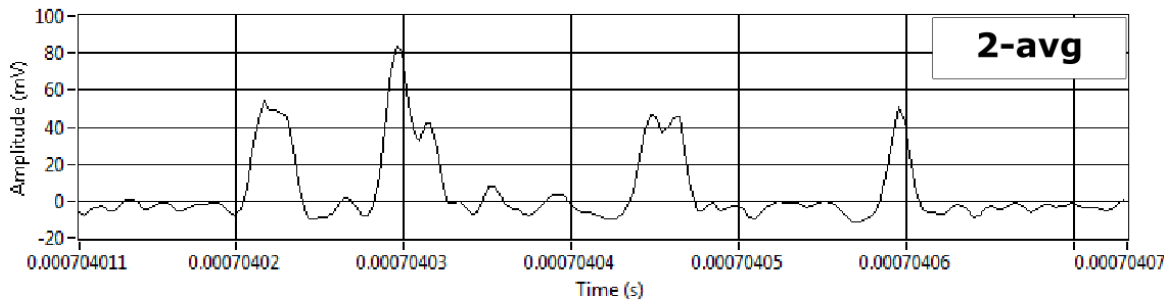


Supplementary Figure 1 KiloHertz frame-rate Imaging of fluorescent proteins-in *ex vivo* mouse brain in layer 2/3 at a depth of $\sim 150\text{-}250\ \mu\text{m}$ below the dura. The mouse was genetically modified to express the fluorescent protein tdTomato (see methods). The four images on the left were taken at a frame-rate of 2kHz and 2-times averaged (i.e. 1ms recording time). The images were spatially binned with 3x3 pixels as only single photons were detected per focal volume (cf. supplementary figure 2). Individual neurons are visible, however low SNR is achieved at these high frame-rates as fluorophore levels were too low and the fluorescent signal was already saturated. The pictures on the right were averaged 200-times, which leads to sufficiently high photon numbers for FLIM (right, last column). Each image pair on the right was acquired within 100ms recording time. Power after the objective was 150mW, i.e. 26W pulse peak power.

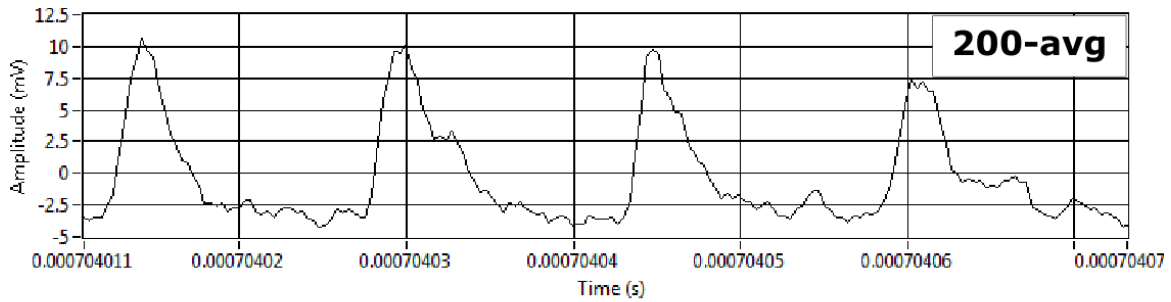


Supplementary Figure 2 Comparison of images between averaging 2-times (left), 200-times (middle) and 2000-times (right). The acquisition times are thus 1ms, 100ms, and 1000ms, respectively. More averaging leads to much increased SNR (see supplementary figure 3) and also permits extracting the lifetime of the tdTomato fluorescence (see supplementary figure 4). On the upper right corner there is a photobleached square visible. This bleaching was caused by the previous imaging position where the sample was imaged for ~ 10 minutes. Power after the objective was 150mW, i.e. 26W pulse peak power.

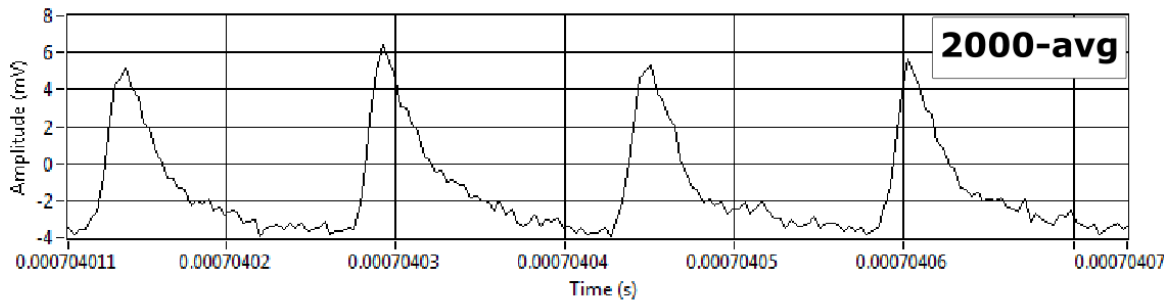
Time Trace Raw



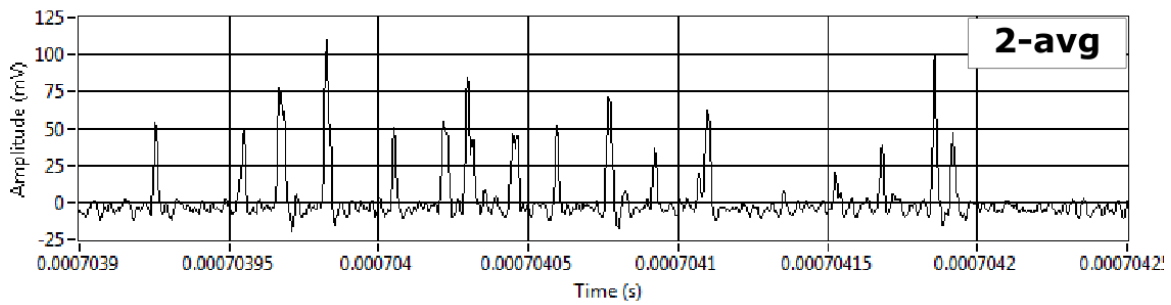
Time Trace Raw



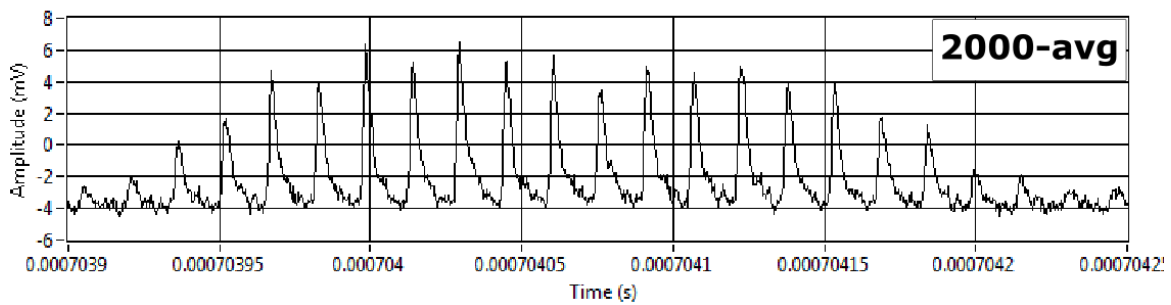
Time Trace Raw



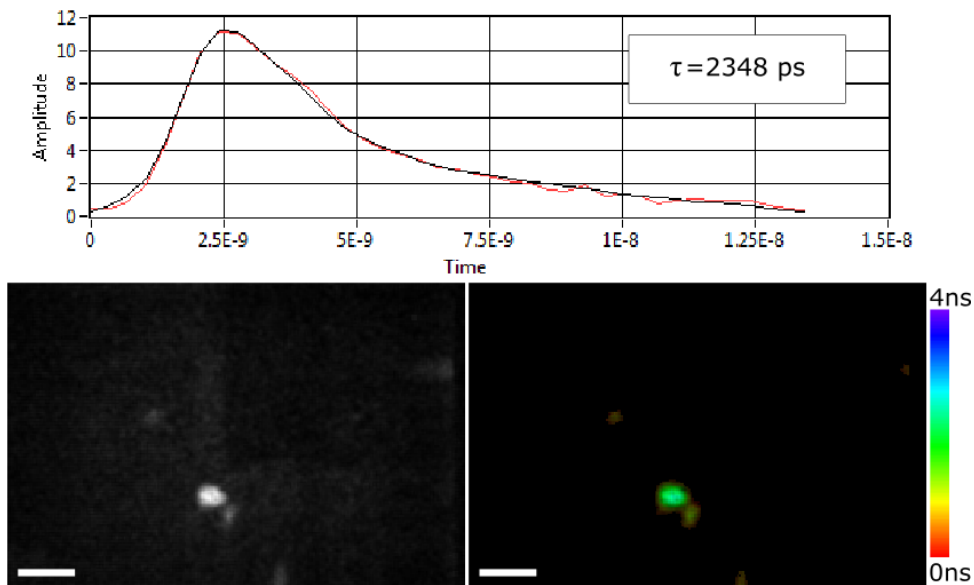
Time Trace Raw



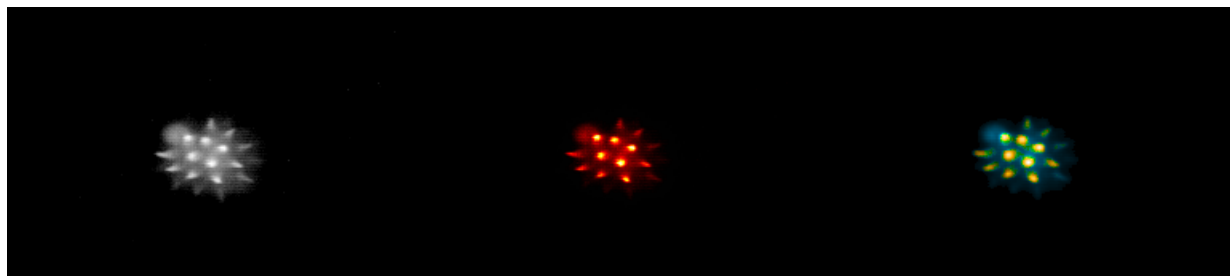
Time Trace Raw



Supplementary Figure 3 Time Traces for the raw fluorescence signal from a tdTomato fluorescing neuron from supplementary figure 2. The 2-times averaged time trace shows individual photons arriving at the detector. In the first image, 8 photons are visible, where each photon generates an amplitude of 50mV and has a temporal width of 1026ps corresponding to the IRF (cf. Fig. 2). The sparsity of the excited fluorescent photons explains the low SNR of the 2-times averaged images in supplementary figures 1 and 2. Only when averaging many frames (200 and 2000-times averaging shown), the ensemble behavior of the fluorescent lifetime decay becomes visible. Thus, for this low concentration of tdTomato fluorescent proteins in the genetically-modified mouse brain the imaging speed of SLIDE of 2 kHz cannot be reached at sufficiently high SNR to permit $\Delta F/F_0$ determination of action potentials.



Supplementary Figure 4 SLIDE images of tdTomato expressing neurons. The lower images represent the TPM image (left) and the FLIM image (right). The frame-rate was 2kHz and 200 images were averaged to reach sufficient photon levels for reliable mono-exponential lifetime fits. The decay data together with a monoexponential, convoluted lifetime fit for a single pixel is shown above yielding a lifetime of 2348ps. The TPM image was 3x3 spatially binned, the FLIM image was 7x7 spatially binned. Scale bars represents 10 μ m. The total acquisition time for the image pair was 100ms, so neuronal imaging with FLIM capability at 10Hz imaging rate seems reasonable with the SLIDE system.



Supplementary Figure 5 Two-Photon Fluorescence and TP-FLIM Images of a Pollen grain. The image to the left is the fluorescence image displayed on a logarithmic scale. The spikey protrusions are on the sub μ m scale and nicely visualize the high spatial resolution of the SLIDE microscope. The middle image is the same image with a "Red Hot" lookup table. The image on the right is the FLIM image where the spikes show a different fluorescent lifetime than the pollen body. The images were 100-times averaged, corresponding to 20Hz video-rate acquisition time for these images.